



HAL
open science

Monte Carlo simulation of free radical production under keV photon irradiation of gold nanoparticle aqueous solution. Part II: Local primary chemical boost

Floriane Poignant, Hela Charfi, Chen-Hui Chan, Elise Dumont, David Loffreda, Benoit Gervais, Michaël Beuve

► To cite this version:

Floriane Poignant, Hela Charfi, Chen-Hui Chan, Elise Dumont, David Loffreda, et al.. Monte Carlo simulation of free radical production under keV photon irradiation of gold nanoparticle aqueous solution. Part II: Local primary chemical boost. *Radiation Physics and Chemistry*, 2021, 179, pp.109161. 10.1016/j.radphyschem.2020.109161 . hal-03029595

HAL Id: hal-03029595

<https://hal.science/hal-03029595>

Submitted on 30 Nov 2020

HAL is a multi-disciplinary open access archive for the deposit and dissemination of scientific research documents, whether they are published or not. The documents may come from teaching and research institutions in France or abroad, or from public or private research centers.

L'archive ouverte pluridisciplinaire **HAL**, est destinée au dépôt et à la diffusion de documents scientifiques de niveau recherche, publiés ou non, émanant des établissements d'enseignement et de recherche français ou étrangers, des laboratoires publics ou privés.

Manuscript Details

Manuscript number RPC_2020_500

Title Monte Carlo simulation of free radical production under keV photon irradiation of gold nanoparticle aqueous solution. Part II: local primary chemical boost.

Abstract

For the past two decades, gold nanoparticles (GNPs) have been investigated as a radiosensitizing agent for radiation therapy. Many theoretical studies have shown that GNPs increase the dose deposition for keV photon irradiation, both at macro and nano-scales, due to a high photon-gold interaction probability. We studied by Monte Carlo simulations the production of radiolysis chemical products (OH and H₂O₂) following an ionization event induced by a 20-90 keV photon in a nanoparticle (NP). We focused here on the primary chemical processes occurring around nanoparticles. In the micrometer range, we obtained an excess of chemical species following GNP ionization, as compared to a reference water nanoparticle (WNP) ionization. This difference came from the dominant processes of photon interaction, i.e., Compton for water and photoelectric for gold, which are characterized by different emitted-electron energy spectra. The overproduction of chemical species could be up to 5 times higher for GNP, depending on the photon energy. The mean concentration of chemical species in a 100 nm sphere is higher for GNPs compared to WNPs due to Auger electrons when the nanoparticle radius was equal to 5 nm. On the contrary, it was quite comparable when the nanoparticle radius was equal to 50 nm. This reveals that gold Auger-electrons do not necessarily induce a significant boost of chemical species in the vicinity of GNP, as compared to WNP. For large GNPs, the local effect (i.e., within a few hundreds of nm from the NP surface) is not to induce a large yield near the ionized GNP, but rather to increase the chance of this event to occur, due to higher photon-gold interaction probability than that of water.

Submission Files Included in this PDF

File Name [File Type]

Highlights.docx [Highlights]

Article_final.pdf [Manuscript File]

To view all the submission files, including those not included in the PDF, click on the manuscript title on your EVISE Homepage, then click 'Download zip file'.

- We calculate free radical production around a gold nanoparticle (GNP) or a water nanoparticle (WNP) in water, for single keV photon absorption.
- In the micrometer range from NP surface, radicals are overproduced of radicals by GNP (photoelectric effect) compared to WNP (Compton scattering).
- In the nanometer range, radicals are overproduced by small GNP compared to WNP due to Auger electrons, and comparable for large NP.

1
2
3
4
5
6
7
8
9
10
11
12
13
14
15
16
17
18
19
20
21
22
23
24
25

Monte Carlo simulation of free radical production under keV photon irradiation of gold nanoparticle aqueous solution. Part II: local primary chemical boost.

13 Floriane Poignant^a, Hela Charfi^a, Chen-Hui Chan^b, Elise Dumont^{b,d}, David
14 Loffreda^b, Benoit Gervais^c, Michaël Beuve^a

^a*Univ. Lyon, Univ. Claude Bernard Lyon 1, CNRS/IN2P3, IP2I Lyon, F-69622,
17 Villeurbanne, France.*

^b*Univ Lyon, Ens de Lyon, CNRS UMR 5182, Université Claude Bernard Lyon 1,
19 Laboratoire de Chimie, F-69342 Lyon, France*

^c*CIMAP, unité mixte CEA-CNRS-ENSICAEN-UCBN 6252 BP 5133, F-14070 Caen,
21 Cedex 05, France*

^d*Institut Universitaire de France, 5 rue Descartes, 75005 Paris*

Abstract

26
27
28
29
30
31
32
33
34
35
36
37
38
39
40
41
42
43
44
45
46
47

For the past two decades, gold nanoparticles (GNPs) have been investigated as a radiosensitizing agent for radiation therapy. Many theoretical studies have shown that GNPs increase the dose deposition for keV photon irradiation, both at macro and nano-scales, due to a high photon-gold interaction probability. We studied by Monte Carlo simulations the production of radiolysis chemical products ($\bullet\text{OH}$ and H_2O_2) following an ionization event induced by a 20-90 keV photon in a nanoparticle (NP). We focused here on the primary chemical processes occurring around nanoparticles. In the micrometer range, we obtained an excess of chemical species following GNP ionization, as compared to a reference water nanoparticle (WNP) ionization. This difference came from the dominant processes of photon interaction, i.e., Compton for water and photoelectric for gold, which are characterized by different emitted-electron energy spectra. The overproduction of chemical species could be up to 5 times higher for GNP, de-

48 *Email address: michael.beuve@univ-lyon1.fr (Michaël Beuve)*

57
58
59
60
61
62
63
64
65
66
67
68
69
70
71
72
73
74
75
76
77
78
79
pending on the photon energy. The mean concentration of chemical species in a 100 nm sphere is higher for GNPs compared to WNPs due to Auger electrons when the nanoparticle radius was equal to 5 nm. On the contrary, it was quite comparable when the nanoparticle radius was equal to 50 nm. This reveals that gold Auger-electrons do not necessarily induce a significant boost of chemical species in the vicinity of GNP, as compared to WNP. For large GNPs, the local effect (i.e., within a few hundreds of nm from the NP surface) is not to induce a large yield near the ionized GNP, but rather to increase the chance of this event to occur, due to higher photon-gold interaction probability than that of water.

Keywords: gold nanoparticles, photon irradiation, water radiolysis, free radical production, Monte Carlo simulation

80 81 82 83 84 85 86 87 88 89 90 91 92 93 94 95 96 97 98 99 100 101 102 103 104 105 106 107 108 109 110 111 112

1. Introduction

Over the past two decades, the use of high-atomic-number (Z) nanoparticles (NPs) has been of high interest due to their radiosensitizing properties. Several pre-clinical studies have shown the efficiency of gold NPs (GNPs) to enhance the effect of radiation therapy, in particular when using low energy (keV) X-rays [1, 2]. The origin of NP enhanced radiotherapy may originate from complex physical, chemical and biological mechanisms. The relative contribution of each stage remains under investigation [3]. Theoretical approaches, such as Monte Carlo (MC) simulations, may help to better understand how early physical and chemical stages could impact a biological system and lead, for instance, to cell death increase.

MC studies have shown that, for keV X-rays, a significant increase of dose deposition may be reached for sufficiently large gold concentration [4, 5]. At such energies, the photo-electric effect dominates for high- Z materials and the photon interaction probability with GNP is much larger than the interaction probability with biological tissues. Other MC studies have suggested that the heterogeneity of dose deposition in the vicinity of NPs may further contribute to the enhancement, due to an hypothetical release of low-energy electrons.

113
114
115
116
117
118
119
120
121
122
123
124
125
126
127
128
129
130
131
132
133
134
135
136
137
138
139
140
141
142
143
144
145
146
147
148
149
150
151
152
153
154
155
156
157
158
159
160
161
162
163
164
165
166
167
168

Following a photo-ionization of a high-Z NP, **desexcitation** processes result in the emission of a cascade of secondary electrons called Auger cascade. It might be responsible for a high energy deposition in the vicinity of the GNP, and has often been associated with GNP efficiency, by presumably inducing an increased biological effectiveness similar to that observed in hadrontherapy [4, 5, 6, 7, 8].

While there have been many MC studies of the physical stage and dose deposition, simulation studies of the chemical stage are scarce [9, 10, 11]. In particular, GNP impact on water radiolysis has hardly been investigated, although it was suggested to be a crucial step that may connect the physical effect to the biological consequences [3]. In a previous work [12], we studied, on a macroscopic scale, the impact of GNPs on free radical yields for 20-90 keV photon irradiation. We showed that for a GNP concentration of $1 \text{ mg} \cdot \text{mL}^{-1}$, the increase of yields is well correlated to the macroscopic dose enhancement. Yields were found to mostly depend on the photon energy and, to a lesser extent, on the NP radius for a given mass concentration of GNPs. As previous MC studies at nanometric scale pointed out the importance of dose heterogeneity and, in particular, the high energy deposition in the vicinity of the GNP [13, 8, 14, 15, 16, 17, 18], we wished to focus, in this study, on the production of chemical species at the nanoscale. In particular we searched for a possible boost of radical production near the GNP, which might lead to local enhancement of radical recombination.

The goal of this work was thus to investigate, in a systematic way, the production of free radicals for keV photon irradiation in water around one GNP, following the absorption of a photon by this nanoparticle. It was compared to the production of chemical species following a photon absorption in a ~~nanoparticle made of water~~ (WNP), to highlight the specificity of gold material. We focused in particular on the production of **oxydative** species (hydroxyl radicals $\bullet\text{OH}$ and hydrogen peroxide H_2O_2). To calculate these chemical species production, we implemented a MC simulation which models the physical, physico-chemical and chemical steps.

This paper is organized as follows. In section 2, the MC tool and simulation

169
170
171
172
173
174
175
176
177
178
179
180
181
182
183
184
185
186
187
188
189
190
191
192
193
194
195
196
197
198
199
200
201
202
203
204
205
206
207
208
209
210
211
212
213
214
215
216
217
218
219
220
221
222
223
224

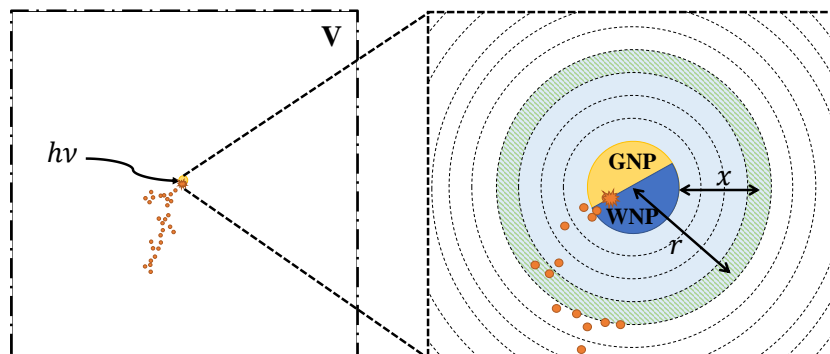


Figure 1: **Schematic view of the geometry.** Orange dots represent excited or ionized water molecules or chemical species produced following the NP ionization. On the right, the dashed green and blue area represents the scoring volume used to calculate radical species concentration in spherical concentric shells, $c_X(x)$ and $C_X(x)$.

geometry are presented. Section 3 presents the radial distribution of chemical
50 species around a NP. Section 4 discusses and concludes on the results.

2. Material and methods

2.1. Geometry

The geometry considered for the calculation is described in Fig. 1. We defined a
GNP placed at the center of a volume V filled with liquid water. The half length
203 of V was chosen to be larger than the maximum range of the most energetic
204 of V was chosen to be larger than the maximum range of the most energetic
55 of V was chosen to be larger than the maximum range of the most energetic
206 photo-electron in water. The GNP was ionized by a photon whose energy varied
207 from 20 to 90 keV. The half length of the volume was hence larger than 160 μm .
208 The systematic study of the NP-size impact on chemical species yields were
209 performed with four NP radii (5 nm, 12.5 nm, 25 nm and 50 nm). To analyze
210 the specificity of gold material, the calculation was also performed for a spherical
211 the specificity of gold material, the calculation was also performed for a spherical
60 the specificity of gold material, the calculation was also performed for a spherical
212 NP made of water with the same radius.
213 NP made of water with the same radius.
214 NP made of water with the same radius.
215 NP made of water with the same radius.
216 NP made of water with the same radius.
217 NP made of water with the same radius.
218 NP made of water with the same radius.
219 NP made of water with the same radius.
220 NP made of water with the same radius.
221 NP made of water with the same radius.
222 NP made of water with the same radius.
223 NP made of water with the same radius.
224 NP made of water with the same radius.

225
226
227
228
229
230
231
232
233
234
235
236
237
238
239
240
241
242
243
244
245
246
247
248
249
250
251
252
253
254
255
256
257
258
259
260
261
262
263
264
265
266
267
268
269
270
271
272
273
274
275
276
277
278
279
280

2.2. Monte Carlo simulation for water radiolysis

Our calculation was based on the Monte Carlo simulation MDM, and the full description of the model is available elsewhere [12, 19, 20]. In short, 3 consecutive stages were performed to calculate the yield of chemical species. The physical stage consisted of an event-by-event tracking of electrons in the different media (water or gold) down to thermalization energy at 300 K (37 meV). Photons were not explicitly tracked, and we only considered the photoelectric effect and the Compton scattering as they dominate at the investigated photon energies. The photon ionization impact was randomly distributed within the NP. At the end of the physical stage, the surrounding water molecule may be found either excited (H_2O^*) or ionized (H_2O^+ , H_2O^{2+} and H_2O^-), and the medium contained thermalized electrons. The electrons in GNP for which the energy was too low to escape the GNP surface were no longer tracked, as they did not lead to additional water molecule excitation or ionization.

This stage was followed by a physico-chemical stage during which the medium relaxes, leading to the production of primary chemical species. The different branching ratios of each molecular rearrangement are given elsewhere [20]. At the end of this stage, the outcome consisted of spatial distribution of chemical species in water, with a majority of e_{aq}^- , H_3O^+ and $\bullet\text{OH}$.

Finally, during the chemical stage, the primary chemical species diffused and interacted with each other. More than 50 chemical reactions were considered. In our simulation, this phase was simulated up to 10^{-6} s. The method used to calculate the yields and to optimize the computing time, as well as the list of standard chemical reactions of water radiolysis, are available elsewhere and will not be discussed in this paper [20, 21, 22, 12]. In this study, we did not consider any possible specific reactions at the surface of the GNP.

2.3. Calculated quantities

We calculated 4 different quantities to characterize the production and distribution of chemical species around one NP. We calculated (1) the mean number

281
282
283
284
285
286
287 of chemical species X following one single ionization event in the NP R_X^1 ; (2)
288 the radial number of chemical species, which is the differential of this number
289 in the radial distance $\frac{\partial R_X^1}{\partial r}$; (3) the radial concentration of the chemical species
290 X , $c_X(r)$, as the concentration of X averaged over the spherical shell of radius
291 r and of thickness δr and centered around the GNP, as represented in dashed
292 95 r and of thickness δr and centered around the GNP, as represented in dashed
293 green and blue in Fig. 1. This quantity is related to the previous one through
294 the relation,
295
296
297

$$298 \quad c_X(r) = \frac{1}{4/3\pi((r^3 + \delta r) - r^3)} \int_r^{r+\delta r} \frac{\partial R_X^1}{\partial r'} dr'. \quad (1)$$

299
300 Finally, we calculated (4) the spherical concentration defined as concentration
301 per ionized NP, averaged over sphere centered on the nanoparticle and limited
302 by the nanoparticle surface on one side, and the radial distance r on the other
303 100 side, as represented in blue in Fig. 1,
304
305
306
307

$$308 \quad C_X(r) = \frac{1}{\frac{4}{3}\pi(r^3 - R_{\text{NP}}^3)} \int_{R_{\text{NP}}}^r \frac{\partial R_X^1}{\partial r'} dr'. \quad (2)$$

309
310 To have a common origin for all NP radii, the results are presented as a function
311 of the distance from NP surface, $x = r - R_{\text{NP}}$. We shall refer to $c_X(r)$ and $C_X(r)$
312 as $c_X(x)$ and $C_X(x)$.
313
314
315

316 105 **3. Results**

317 *3.1. Average number of chemical species per nanoparticle ionization*

318
319 Tab. 1 gives the average number of chemical species ($R_{\bullet\text{OH}}^1$ and $R_{\text{H}_2\text{O}_2}^1$) for
320 various E_{photon} , two NP radii ($R_{\text{NP}} = 5$ and 50 nm), calculated both at 10^{-12}
321 and 10^{-6} s following the photon absorption.
322
323
324

325 110 For the smallest GNPs, the number of $\bullet\text{OH}$ produced at 10^{-12} s varied from 721
326 ($E_{\text{photon}} = 20$ keV), up to 2912 ($E_{\text{photon}} = 70$ keV), due to the increase of the
327 photo-electron energy. It then dropped at $E_{\text{photon}} = 90$ keV, as there is a high
328 fluorescence emission in this case. The mean free path of the emitted photons is
329
330

337
338
339
340
341
342
343 very large compared to the volume of the simulated system and the probability
344
115 of interaction is low. This latter was neglected in our simulations. If the GNP
346 was embedded in a volume of water larger than the photon mean free path, the
347 photon would deposit its energy in the volume, but most of the time far away
348 (several mm at least) from the ionized GNP. The same variation of $R_{\bullet\text{OH}}^1$ and
349 $R_{\text{H}_2\text{O}_2}^1$ was obtained with regard to E_{photon} , regardless of other parameters (e.g.,
350
351
120 radius, time ...). The number of chemical species decreased with increasing GNP
353 radius due to the energy loss in the GNP. This was particularly visible at 20
354 keV: at 10^{-12} s, the number of $\bullet\text{OH}$ decreased from 721 to 571 when the radius
355 of the GNP increased from 5 nm to 50 nm. The same trends were observed with
356
357 H_2O_2 .
358

359
125 For WNP, the number of chemical species was hardly impacted by the NP size.
360 The number of chemical species, at fixed time, first decreased from 20 keV to
361 50 keV, before increasing again. The first drop was due to the fact that, at
362 20 keV, the photo-electric effect remained non-negligible, in which case all the
363 photon energy was deposited. As the Compton effect became dominant, only
364
365
130 part of the photon energy was deposited. This was compensated by the fact
366 that the average Compton electron energy increased with the photon energy, so
367 that the number of species per photo-ionization increased above 50 keV.
368
369

370 The number of chemical species generated per photo-ionization was systemati-
371 cally higher for GNPs than WNPs, with two exceptions. For $E_{\text{photon}} = 20$ keV
372
373
135 and $R_{\text{NP}} = 50$ nm, the number of chemical species for GNPs was below that of
374 WNP, due to a particularly high energy absorption within the GNP. At 10^{-6} s,
375 $E_{\text{photon}} = 20\text{keV}$, $R_{\text{NP}} = 5$ nm, and regardless of the time, the number of $\bullet\text{OH}$
376 for GNP was also below that of WNP, while it was not the case of H_2O_2 . This
377 denotes the fact that in this specific case, the recombination of $\bullet\text{OH}$ was par-
378 ticularly important, leading to a high number of H_2O_2 . Finally, as expected,
379
140 the largest difference between GNPs and WNPs was obtained at 70 keV. In this
381 case, the photo-electron emitted from the GNP had the largest kinetic energy,
382 while the Compton electron in water still had a limited kinetic energy.
383
384
385
386
387
388
389
390
391
392

393
394
395
396
397
398
399
400
401
402
403
404
405
406
407
408
409
410
411
412
413
414
415
416
417
418
419
420
421
422
423
424
425
426
427
428
429
430
431
432
433
434
435
436
437
438
439
440
441
442
443
444
445
446
447
448

Energy	10^{-12} s				10^{-6} s			
	•OH		H ₂ O ₂		•OH		H ₂ O ₂	
	GNP	WNP	GNP	WNP	GNP	WNP	GNP	WNP
	$R_{\text{NP}} = 5$ nm							
20 keV	721	673	33	28	256	288	135	118
50 keV	2070	460	81	20	934	198	350	81
70 keV	2912	501	112	21	1385	211	482	88
90 keV	1560	618	63	25	671	264	270	108
	$R_{\text{NP}} = 50$ nm							
20 keV	571	674	25	28	212	288	107	118
50 keV	1960	455	76	19	906	196	329	80
70 keV	2820	500	107	21	1365	211	462	88
90 keV	1401	617	56	26	625	263	239	108

Table 1: Average number of chemical species produced per GNP/WNP ionization for different times, photon energies and GNP radii. The statistical uncertainty was below 1 %.

3.2. Spatial distribution

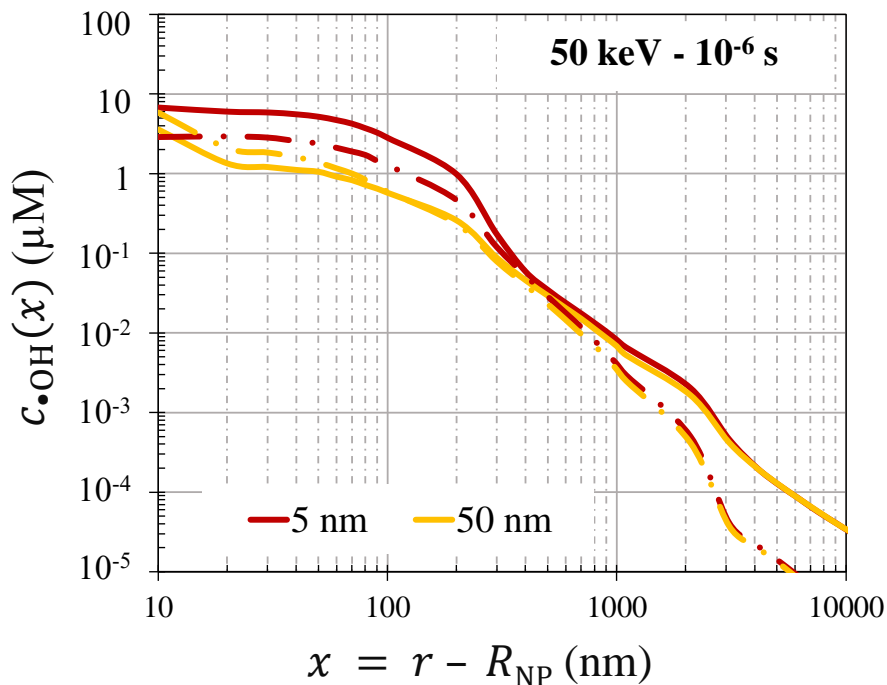


Figure 2: Radial concentration $c_{\bullet\text{OH}}(x)$ as a function of x ($E_{\text{photon}} = 50$ keV and $t = 10^{-6}$), for two R_{NP} . Solid line shows results for a GNP and dashed line for a WNP.

Fig. 2 shows the radial concentration $c_{\bullet\text{OH}}(x)$ of $\bullet\text{OH}$ following an ionization event in the NP, as a function of the distance to the NP surface $x = r - R_{\text{NP}}$.

The radial concentration was maximum near the NP surface and dropped severely for higher values of r . This decrease was proportional to $1/r^2$. It is due to the dependency in r^2 of spherical shell volume when r increases, and to a lesser extent to the differential number of chemical species. Such tendency was similar regardless of the photon energy, both at 10^{-12} s (not shown here) and 10^{-6} s. The global shape of the radial distribution was not specific to the material, as WNP showed the same tendency.

Due to $\bullet\text{OH}$ recombination and diffusion, the radial concentration decreased

505
506
507
508
509
510
511
512 with increasing t over the whole r range for $\bullet\text{OH}$. For H_2O_2 (not shown here),
513 $c_{\text{H}_2\text{O}_2}(x)$ dropped for $x < 200$ nm over the time period 10^{-12} to 10^{-6} . This
514 drop was due to outward diffusion, which is of the order of 100 nm for 1 μs . On
515 the contrary, H_2O_2 increased for larger radii.
516

517
518 Increasing the NP radius R_{NP} decreased $c_{\bullet\text{OH}}(x)$ below 200 nm, regardless of
519 photon energy, time t , chemical species or material. There are two reasons for
520 this. First, by definition of the radial concentration, the number of species is
521 normalized to the volume of the shell. For a given value of x , this volume
522 increases with increasing R_{NP} . Second, the part of the absorbed energy inside
523 the NP, which increases with increasing R_{NP} , corresponds to the stopping of
524 low-energy electrons. When increasing the NP radius, less low-energy electrons
525 escape the NP and less species are produced close to the surface.
526
527
528

529 The spatial distribution of chemical species also depended on photon energy.
530 To better analyze this dependency, we calculated the radial number of chemical
531 species, instead of the radial concentration as the latter was strongly impacted
532 by the r^2 normalization. Fig. 3 displays the radial number of chemical species
533 $\bullet\text{OH}$, $\frac{\partial R_{\bullet\text{OH}}^1}{\partial r}$, as a function of the distance to the NP surface x .
534
535

536 For GNP, some structures are visible around $x = 100$ nm and 1000 nm, regard-
537 less of the photon energy. The first structure came from LLS ($S > N$) Auger
538 electrons emitted with an energy lower than 2 keV, which had ranges lower than
539 ~ 160 nm in water. The second structure came from LMS ($S > M$) Auger elec-
540 trons emitted with an energy between 8-12 keV, which corresponded to a range
541 in water around 1000-2000 nm. Another structure is visible for large x , which
542 corresponded to the end of photo-electron path. As shown in Tab. 2, these
543 photo-electrons have different energies depending on the photon energy and the
544 shell from which they are ejected. This phenomenon was particularly visible for
545 $E_{\text{photon}} = 90$ keV. As the probability to ionize the K-shell was overwhelming
546 in this case, many photo-electrons were ejected with an energy around 9 keV.
547 These electrons therefore contributed to the boost of the number of chemical
548 species observed around 1000 nm.
549
550
551
552
553
554

561
562
563
564
565
566
567
568
569
570
571
572
573
574
575
576
577
578
579
580
581
582
583
584
585
586
587
588
589
590
591
592
593
594
595
596
597
598
599
600
601
602
603
604
605
606
607
608
609
610
611
612
613
614
615
616

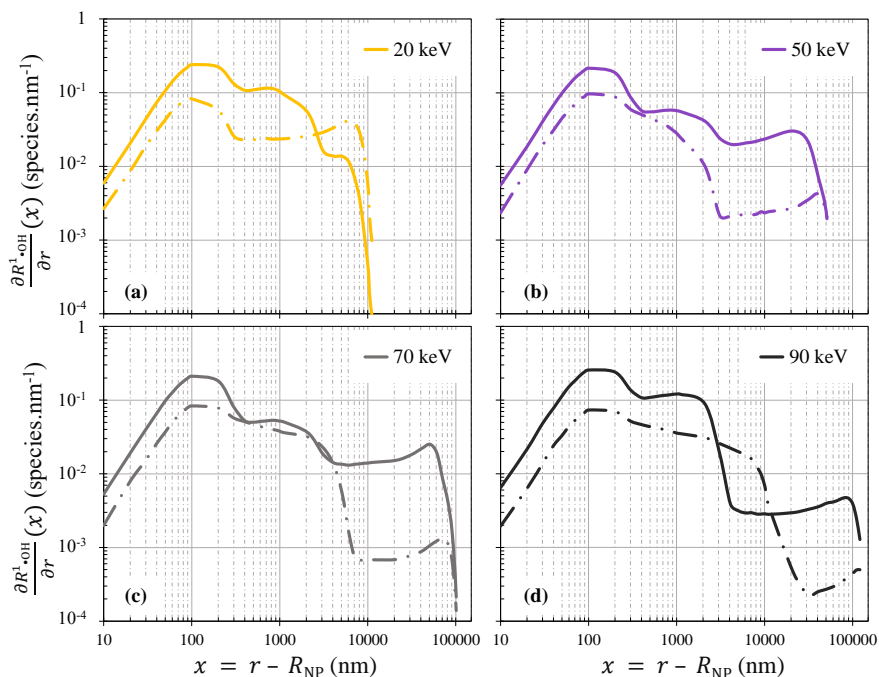


Figure 3: Radial number of chemical species $\frac{\partial R_{\bullet}^{\text{OH}}}{\partial r}$ as a function of x . In each panel, results are given for GNP (solid line) and WNP (dashed line). Results are displayed for $E_{\text{photon}} = 20, 50, 70$ and 90 keV. $R_{\text{NP}} = 5$ nm, and $t = 10^{-6}$ s.

185 For WNP, the progressive decrease of $\frac{\partial R_{\bullet}^{\text{OH}}}{\partial r}$ with x was related to the energy
 594 distribution of Compton electrons. An exception was noticeable for 20 keV: as
 595 the photo-electric effect remained non-negligible, the radial number of chemi-
 596 cal species was a combination of the radial number following a photo-electric
 597 event producing a ~ 19.5 keV photo-electron, and the radial number following
 598 a Compton event producing a broad energy distribution below 1400 eV.
 190

602 When comparing GNP and WNP, the first striking fact was that $\frac{\partial R_{\bullet}^{\text{OH}}}{\partial r}$ re-
 603 mained higher at longer distances ($x > \sim 10\,000$ nm) for GNP. This is explained
 604 by the fact that, on average, the Compton electron had an energy lower than
 605 a photo-electron energy. At very small distance ($x < 100$ nm), the number of
 606 chemical species was higher for GNP compared to WNP when $R_{\text{NP}} = 5$ nm.
 195 On the contrary, it was lower for GNP compared to WNP when $R_{\text{NP}} = 50$ nm.

h

Atomic shell	K			L			≥ M		
	E_{photon}	P.	E.	R.	P.	E.	R.	P.	E.
20 keV	0	-	-	77	6-8	0.9-1.5	23	> 17	5.3-7.4
50 keV	0	-	-	77	17-18	5.3-6	23	> 47	35-42
70 keV	0	-	-	77	56-58	49-53	23	> 67	68-74
90 keV	77	9	1.8	16	76-78	88-92	7	> 87	> 111

Table 2: **Probability** (P. in %) of ionizing the shell K,L or above, photo-electron energy (E. in keV) and range of the photo-electron in water (R. in μm) following an ionization event in gold with a photon of energy E_{photon} .

To better quantify the relative difference between GNP and WNP, we calculated the difference of spherical concentration of GNP and WNP, to that of WNP,

$$\frac{C_{X,\text{GNP}}(x) - C_{X,\text{WNP}}(x)}{C_{X,\text{WNP}}(x)}, \quad (3)$$

for the two extrema sizes of NPs investigated here. Results are shown in Tab. 3
 200 for $\bullet\text{OH}$. The results confirmed that, for $R_{\text{NP}} = 50$ nm, the spherical concentration of WNP for small volumes (10 and 100 nm thick) were higher than that of GNP, except when the photon energy was equal to 90 keV. This was due to non negligible energy loss in the GNP. When the considered volume increased ($x = 1000$ nm), the concentration for GNPs was higher than that of WNP. For
 205 even larger volumes ($x = 10$ μm), the concentrations were higher for GNPs, with one exception ($E_{\text{photon}} = 20$ keV). This translated the fact that, on average, GNPs generated more chemical species than WNP following one photon ionization event, but far away from the GNP (i.e., beyond 100 nm).

4. Discussion and conclusion

210 In this work, we investigated the production and spatial distribution of radical species following keV-photon ionization of a GNP or a WNP embedded in a volume of water. We focus on the local production of radicals, meaning that

673
674
675
676
677
678
679
680
681
682
683
684
685
686
687
688
689
690
691
692
693
694
695
696
697
698
699
700
701
702
703
704
705
706
707
708
709
710
711
712
713
714
715
716
717
718
719
720
721
722
723
724
725
726
727
728

x	10 nm	100 nm	1 000 nm	10 000 nm	100 000 nm
$t = 10^{-6}$ s - $R_{\text{NP}} = 5$ nm					
20 keV	122	164	327	-11	-11
50 keV	137	123	68	289	354
70 keV	165	154	53	77	561
90 keV	233	248	196	30	159
$t = 10^{-6}$ s - $R_{\text{NP}} = 50$ nm					
20 keV	-9	39	238	-26	-26
50 keV	-39	-22	25	264	365
70 keV	-33	-15	9	57	547
90 keV	18	55	152	8	134

Table 3: Relative difference (in %) of spherical $\bullet\text{OH}$ concentration in a x nm thick shell around a nanoparticle.

Compton and fluorescence photons, which release their energy at least millimeters away from the NP, were not taken into account. Radial concentrations showed a high maximum near the nanoparticle surface which rapidly decreased when the distance to the nanoparticle increased. This is a purely geometric effect due to the r^2 increase of the concentric shells used as scoring volume. As a consequence, both GNPs and WNPs showed very similar radial concentration profiles.

Different specificities were obtained for gold compared to water:

(1) We observed that, on average, a GNP ionization can produce up to ~ 5.5 more chemical species than an ionization event in a WNP, as a photo-electron carries more energy than a Compton electron, the later dominating photon-water interactions at the investigated energy. Besides, as photo-electrons are more energetic than Compton electrons, GNP radial concentrations are higher than WNP radial concentrations at distances larger than few micrometers.

(2) Chemical species produced by the interaction of Auger-electrons with water

729
730
731
732
733
734
735 molecules following an ionization event in GNPs induced a minor boost in the
736 radial number. This boost appeared around 100 nm and 1000 nm.

738
739 230 (3) Both $\bullet\text{OH}$ and H_2O_2 had very similar distributions. In particular, H_2O_2
740 production was not particularly higher due to Auger electrons. The Auger
741 electrons are indeed significant for GNP ionization, but their effect is rather
742 comparable to that of Compton electrons produced by WNP ionization.

744
745 (4) The concentration of chemical species was not necessarily higher for GNP
746 compared to WNP near the ionized NP (within a few hundreds of nm), despite
747 235 the Auger electron cascade when the GNP was large. The absorption of low-
748 energy electrons within the GNP produced a drop of the number of chemical
749 species near the surface with respect to the case of smaller GNPs.
750

752 Attempting an extension of these results to biological systems, one may expect
753 240 that, on average, a cellular target containing or located near a large ionized
754 GNP ($x < 200$ nm) does not suffer a higher concentration of chemical species,
755 compared to the ionization of a water molecule. However, it may experience a
756 higher occurrence of this event, as the cross section for gold-photon interaction
757 is higher than that of water-photon interaction at these energies. In other words,
758
759 the major effect of gold is not to induce a high concentration boost of chemical
760 245 species compared to water, but rather to increase the chances of having an
761 ionization, due to a high probability of photon-gold interaction compared to
762 photon-water interaction.
763
764
765

766 In interpreting our results from a biological perspective, it is important to keep
767 250 in mind that biological media contain many scavenging elements. Besides,
768 cells might catalyse complex reactions inducing an additional boost of chem-
769 ical species production. Our calculation may therefore only characterize the
770 primary chemical events at very short time generated by one photo-ionization
771 event. *In vitro* data showed that GNPs often appear clustered together in vesi-
772 cles [23, 24, 25, 26, 27], which might roughly be represented by large GNPs.
773 255
774 Our calculated spherical concentrations may be used to estimate the primary
775
776
777
778

785
786
787
788
789
790
791 chemical boost experienced by cellular components when they internalize GNPs.
792 Typically, a size of 10 nm may represent the dimension of a membrane; a size of
793 100 nm may represent the dimensions of an organelle (mitochondria, lysosome);
794
795
260 a size of 1000 nm may represent the dimensions of a large organelle (large lyso-
796 some); a size of 10 000 nm may represent a nucleus. As our calculation showed,
797 the number of chemical species following an ionization event decreases for large
798 GNPs, especially in its vicinity. At first sight, it thus appears less advantageous
799 to have aggregates rather than isolated GNPs. However, if GNPs accumulate
800
801
802
265 in a specific zone of the cell, an accumulation of damages may occur near the
803 GNPs, due to a high probability of photon-gold interaction. Such accumulation
804 might be deleterious for the cell.
805
806
807

808 **5. Acknowledgment**

809
810 This work was supported by the LABEX PRIMES (ANR-11-LABX-0063) of
811
812
270 Université de Lyon, within the program "Investissements d'Avenir" (ANR-11-
813 IDEX-0007) operated by the French National Research Agency (ANR). This
814 work has been supported by the Fondation ARC pour la recherche sur le cancer.
815 The authors thank Jean-Michel Moreau for his precious help.
816
817

818 **References**

- 819
820
275 [1] J. F. Hainfeld, D. N. Slatkin, H. M. Smilowitz, The use of gold nanoparticles
821 to enhance radiotherapy in mice, *Physics in Medicine & Biology* 49 (18)
822 (2004) N309.
823
824
825 [2] S. Her, D. A. Jaffray, C. Allen, Gold nanoparticles for applications in can-
826 cer radiotherapy: Mechanisms and recent advancements, *Advanced drug*
827
280 *delivery reviews* 109 (2017) 84–101.
828
829
830 [3] E. Brun, C. Sicard-Roselli, Actual questions raised by nanoparticle ra-
831 diosensitization, *Radiation Physics and Chemistry* 128 (2016) 134–142.
832
833
834

- 841
842
843
844
845
846
847
848
849
850
285
851
852
853
854
855
856
857
858
859
860
861
862
863
864
865
866
295
867
868
869
870
871
872
873
874
300
875
876
877
878
879
880
881
882
883
884
885
886
887
888
889
310
890
891
892
893
894
895
896
- [4] S. H. Cho, Estimation of tumour dose enhancement due to gold nanoparticles during typical radiation treatments: a preliminary Monte Carlo study, *Physics in Medicine & Biology* 50 (15) (2005) N163.
- [5] S. H. Cho, B. L. Jones, S. Krishnan, The dosimetric feasibility of gold nanoparticle-aided radiation therapy (GNRT) via brachytherapy using low-energy gamma-/x-ray sources, *Physics in Medicine & Biology* 54 (16) (2009) 4889.
- [6] S. J. McMahon, W. B. Hyland, M. F. Muir, J. A. Coulter, S. Jain, K. T. Butterworth, G. Schettino, G. R. Dickson, A. R. Hounsell, J. M. O Sullivan, et al., Nanodosimetric effects of gold nanoparticles in megavoltage radiation therapy, *Radiotherapy and Oncology* 100 (3) (2011) 412–416.
- [7] S. J. McMahon, W. Hyland, M. Muir, et al., Biological consequences of nanoscale energy deposition near irradiated heavy atom nanoparticles, *Scientific report* 1 (2011) 18.
- [8] E. Lechtman, S. Mashouf, N. Chattopadhyay, B. Keller, P. Lai, Z. Cai, R. Reilly, J. Pignol, A Monte Carlo-based model of gold nanoparticle radiosensitization accounting for increased radiobiological effectiveness, *Physics in Medicine & Biology* 58 (10) (2013) 3075.
- [9] W. Xie, W. Friedland, W. Li, C. Li, U. Oeh, R. Qiu, J. Li, C. Hoeschen, Simulation on the molecular radiosensitization effect of gold nanoparticles in cells irradiated by x-rays, *Physics in Medicine & Biology* 60 (16) (2015) 6195.
- [10] H. Tran, M. Karamitros, V. Ivanchenko, S. Guatelli, S. McKinnon, K. Murakami, T. Sasaki, S. Okada, M. Bordage, Z. Francis, et al., Geant4 Monte Carlo simulation of absorbed dose and radiolysis yields enhancement from a gold nanoparticle under MeV proton irradiation, *Nuclear Instruments and Methods in Physics Research Section B: Beam Interactions with Materials and Atoms* 373 (2016) 126–139.

- 897
898
899
900
901
902
903
904
905
906
907
908
909
910
911
912
913
914
915
916
917
918
919
920
921
922
923
924
925
926
927
928
929
930
931
932
933
934
935
936
937
938
939
940
941
942
943
944
945
946
947
948
949
950
951
952
- [11] B. Rudek, A. McNamara, J. Ramos-Méndez, H. Byrne, Z. Kuncic, J. Schuermann, Radio-enhancement by gold nanoparticles and their impact on water radiolysis for x-ray, proton and carbon-ion beams, *Physics in Medicine & Biology* 64 (17) (2019) 175005.
- 315 [12] F. Poignant, H. Charfi, C.-H. Chan, E. Dumont, D. Loffreda, É. Testa, B. Gervais, M. Beuve, Monte Carlo simulation of free radical production under keV photon irradiation of gold nanoparticle aqueous solution. Part I: Global primary chemical boost, *Radiation Physics and Chemistry* (2020) 108790.
- 320 [13] S. J. McMahon, W. B. Hyland, E. Brun, K. T. Butterworth, J. A. Coulter, T. Douki, D. G. Hirst, S. Jain, A. P. Kavanagh, Z. Krpetic, et al., Energy dependence of gold nanoparticle radiosensitization in plasmid DNA, *The Journal of Physical Chemistry C* 115 (41) (2011) 20160–20167.
- [14] P. Zygmanski, B. Liu, P. Tsiamas, F. Cifter, M. Petersheim, J. Hesser, 325 E. Sajo, Dependence of Monte Carlo microdosimetric computations on the simulation geometry of gold nanoparticles, *Physics in Medicine & Biology* 58 (22) (2013) 7961.
- [15] Y. Lin, H. Paganetti, S. J. McMahon, J. Schuermann, Gold nanoparticle induced vasculature damage in radiotherapy: comparing protons, mega- 330 voltage photons, and kilovoltage photons, *Medical physics* 42 (10) (2015) 5890–5902.
- [16] M. P. Martinov, R. M. Thomson, Heterogeneous multiscale Monte Carlo simulations for gold nanoparticle radiosensitization, *Medical physics* 44 (2) (2017) 644–653.
- 335 [17] P. Zygmanski, E. Sajo, Nanoscale radiation transport and clinical beam modeling for gold nanoparticle dose enhanced radiotherapy (GNPT) using X-rays, *The British journal of radiology* 89 (1059) (2016) 20150200.

- 953
954
955
956
957
958
959
960
961
962
340 963
964
965
966
967
968
969
970
971
972
973
974
975
976
977
978
350 979
980
981
982
983
984
985
986
355 987
988
989
990
991
992
993
994
995
996
997
998
999
1000
1001
1002
1003
1004
1005
1006
1007
1008
- [18] D. Sakata, I. Kyriakou, S. Okada, H. N. Tran, N. Lampe, S. Guatelli, M.-C. Bordage, V. Ivanchenko, K. Murakami, T. Sasaki, et al., Geant4-DNA track-structure simulations for gold nanoparticles: The importance of electron discrete models in nanometer volumes, *Medical physics* 45 (5) (2018) 2230–2242.
- [19] F. Poignant, A. Ipatov, O. Chakchir, P.-J. Lartaud, É. Testa, B. Gervais, M. Beuve, Theoretical derivation and benchmarking of cross sections for low-energy electron transport in gold, *The European Physical Journal Plus* 135 (4) (2020) 358.
- [20] B. Gervais, M. Beuve, G. Olivera, M. Galassi, Numerical simulation of multiple ionization and high LET effects in liquid water radiolysis, *Radiation Physics and Chemistry* 75 (2006) 495–513.
- [21] A. Colliaux, B. Gervais, C. Rodriguez-Lafrasse, M. Beuve, O₂ and glutathione effects on water radiolysis: a simulation study, in: *Journal of Physics: Conference Series*, Vol. 261, IOP Publishing, 2011, p. 012007.
- [22] A. Colliaux, B. Gervais, C. Rodriguez-Lafrasse, M. Beuve, Simulation of ion-induced water radiolysis in different conditions of oxygenation, *Nuclear Instruments and Methods in Physics Research Section B: Beam Interactions with Materials and Atoms* 365 (2015) 596–605.
- [23] B. D. Chithrani, A. A. Ghazani, W. C. Chan, Determining the size and shape dependence of gold nanoparticle uptake into mammalian cells, *Nano letters* 6 (4) (2006) 662–668.
- [24] D. B. Chithrani, S. Jelveh, F. Jalali, M. van Prooijen, C. Allen, R. G. Bristow, R. P. Hill, D. A. Jaffray, Gold nanoparticles as radiation sensitizers in cancer therapy, *Radiation research* 173 (6) (2010) 719–728.
- [25] L. Bobyk, M. Edouard, P. Deman, M. Vautrin, K. Pernet-Gallay, J. Delaroche, J.-F. Adam, F. Estève, J.-L. Ravanat, H. Elleaume, Photoactiva-

1009
1010
1011
1012
1013
1014
1015
1016
1017
1018
1019
1020
1021
1022
1023
1024
1025
1026
1027
1028
1029
1030
1031
1032
1033
1034
1035
1036
1037
1038
1039
1040
1041
1042
1043
1044
1045
1046
1047
1048
1049
1050
1051
1052
1053
1054
1055
1056
1057
1058
1059
1060
1061
1062
1063
1064

365 tion of gold nanoparticles for glioma treatment, *Nanomedicine: Nanotech-*
1016 *nology, Biology and Medicine* 9 (7) (2013) 1089–1097.

[26] J. Jeynes, M. Merchant, A. Spindler, A. Wera, K. Kirkby, Investigation of
1020 gold nanoparticle radiosensitization mechanisms using a free radical scav-
1021 enger and protons of different energies, *Physics in Medicine & Biology*
1022 59 (21) (2014) 6431.

370 [27] P. Retif, A. Reinhard, H. Paquot, V. Jouan-Hureau, A. Chateau,
1026 L. Sancey, M. Barberi-Heyob, S. Pinel, T. Bastogne, Monte Carlo simu-
1027 lations guided by imaging to predict the in vitro ranking of radiosensitizing
1028 nanoparticles, *International journal of nanomedicine* 11 (2016) 6169.